THREE-DIMENSIONAL FOCUSING SCHLIEREN USING A PLENOPTIC CAMERA

Philipp Kerth, Tobias Hermann, Matthew McGilvray

University of Oxford, Department of Engineering Science, Oxford Thermofluids Institute

ABSTRACT

Many flows involve 3D density changes. These density changes can be qualitatively measured by optical imaging techniques such as schlieren imaging. In order to improve flow visualization a focusing schlieren system with three-dimensional imaging ability is developed. The technology of a plenoptic camera allows to capture 3D information with a single photograph by recording the incident angle of incoming light rays. A plenoptic focusing schlieren system is set up and characterized to be able to resolve more than 25 focal planes in depth direction. The application of focus measures allows to infer simple 3D information from a focal stack generated by the post processing software. More complex 3D information is obtained by measuring the optical impulse response, the so-called point spread function. This is used to perform a full 3D reconstruction of flow objects from a single schlieren photograph.

Index Terms— Plenoptic Imaging, Schlieren, 3D Flow

1. INTRODUCTION

Schlieren photography, an optical technique for flow visualization, was invented more than 150 years ago [1], and has proven to be a powerful tool in experimental aerospace engineering. In the 1990s, Weinstein revived and finalized the focusing schlieren system (Figure 1) [1]–[3]. By moving a lens, this system allows measurement of 3D information taking multiple photographs [2], [4]. This is possible due to a very narrow depth of field. However, this would require the ability to take multiple photos of the exact same flow object and would limit the application to absolutely steady phenomena. An example is provided by Vaisakh and Muruganandam [4], who successfully reconstructed 3D information about a supersonic shock from a focusing schlieren system with deconvolution algorithms. However, to obtain the volumetric data, they had to traverse the entire optical system while taking multiple images and herein relied on the time-invariant nature of their flow phenomena [4].

The invention of plenoptic cameras could allow further adaptation to obtain 3D information from one photo [5]. A 4D light field is captured by those devices, allowing to trace the direction of light rays and eventually reconstruct 3D information [6]. In this work, reconstruction and deconvolution algorithms from biomedical imaging are modified and used to obtain a full volume reconstruction [5] of focusing schlieren images.

The first successful application of plenoptic imaging to semitransparent objects was conducted by Levoy *et al.* [5]. After the application to biomedical microscopy, related work has been done by Fahringer *et al.* [7] who used a plenoptic camera for particle image velocimetry and reconstructed a flow field. The same research team around Klemkowsky *et al.* [8] presented a plenoptic background oriented schlieren system in 2017 successfully applying refocusing and measuring a four-dimensional displacement field. Without adding any additional optics Eberhart and Loehle applied a plenoptic camera to photography of low-density plasma flows revealing a 3D structure of a jet [9]. Ahmed and Wiley [10] have presented a light field focusing schlieren system and it has been used by Ozawa et al. [11] to obtain 3D information about a supersonic shock, wherein they gained the ability to re-focus and minimize depth of field from using multiple light sources in a certain spatial arrangement. In this work, we largely follow the approach from [10]. However, our `plenoptic component' is the camera rather than the LEDs and we present a full 3D reconstruction of flow phenomena. We thus augment the approach from [10] and add another method to the schlieren imaging family. The paper shows how schlieren images are recorded with a plenoptic camera, the performance of the imaging system and its capabilities are characterized, and it explains the concept of plenoptic imaging and how basic 3D information can be inferred by quantitatively analyzing the focus in a set of images.

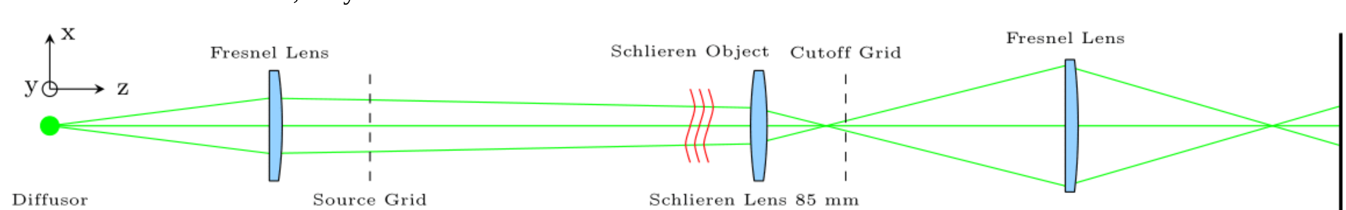

Figure 1*: Focusing schlieren system.*

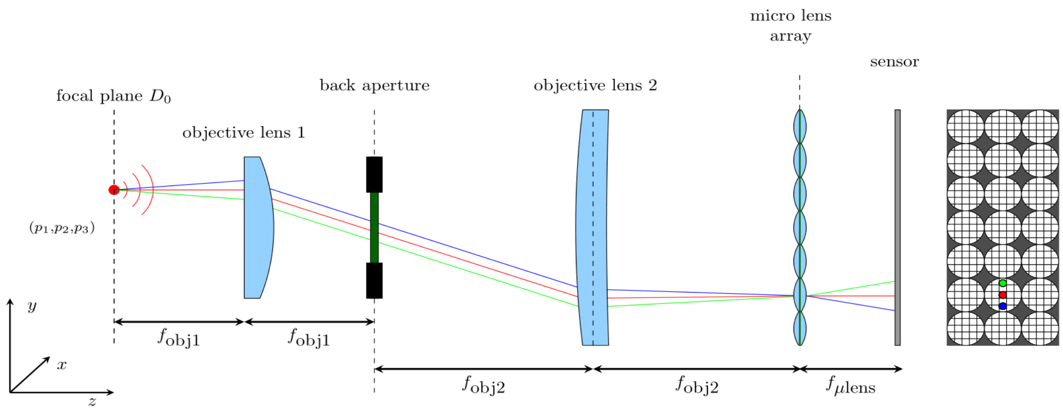

Figure 2*: Geometrical optics of a plenoptic camera. The focal lengths are indicated as f. Adapted from* [32] *with permission.*

Eventually, a full 3D reconstruction of a proof-of-concept experiment where gas is flowing out of two tubes is shown.

2. FOCUSING SCHLIEREN SYSTEM

The physical concept of schlieren imaging lies in the dependency of the refractive index n on the density of a fluid ρ [1]. This is described by Equation 1 where k is the Gladstone- Dale coefficient which is approximately 0.23 cm^3/g for air [1].

$$n - 1 = k\rho \qquad (1)$$

If the density changes, a light ray propagating in z-direction (Coordinates follow the configurations given in Figure 1 and Figure 2) passing through the fluid will be deflected by and angle ϵ in direction i which can be calculated by: [1]

$$\epsilon_i = \frac{1}{n}\int \frac{\partial n}{\partial i}\partial z, \;\; i \in \{x, y\} \qquad (2)$$

All the components of the optical setup are schematically shown in Figure 1. In our focusing schlieren system a LED illuminates a diffusor, which removes all previous focus and provides a homogeneous light source [5]. The source grid pattern is imaged onto a photographic inverse pattern, called the cutoff grid [2] following the exact scheme demonstrated by Weinstein [2]. According to Equation 2, a change in refractive index caused by a change in gas density (Equation 1) inside the test volume causes this pattern to be deflected from its original path [2]. As a result, a deviation from the normal light throughput intensity is caused by a cutoff which can be imaged by a camera [1], [2]. Due to the preliminary focus provided by the first Fresnel lens and the schlieren lens only deflections from a specific plane inside the test volume cause a significant enough change in intensity to be imaged. Hence, the system is `focused' – as its name implies - and only density gradients at a specific depth are imaged sharply [2].

3. LIGHT FIELD DEFINITION

The 4D light field is usually written as $L_{D_0}(x, y, u, v)$ and can be fully defined and depicted using the 2-plane parameterization as shown in Figure 3 [12]–[14]. Upon capturing an image, a camera loses spatial information [12]. Mathematically, this yields the ``photography operator''[12] (Equation 3) [15] as an integral over the aperture surface. The integrand is the light field sampled at the focal plane D_0 as shown in Figure 2 [12]. However, a plenoptic camera is able to measure both coordinate sets (x,y and u,v), thus recording the full 4D light field inside the camera [8], [12].

$$E(x, y) = \int\int L_{D_0}(x, y, u, v) cos^4(\phi) \mathrm{d}u\mathrm{d}v \qquad (3)$$

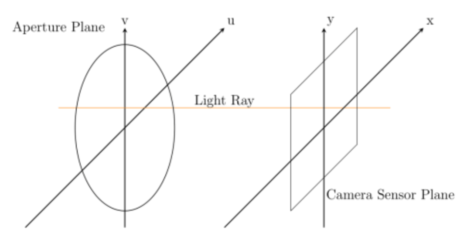

Figure 3*: Light field inside a camera adapted from* [12]. *The two-plane parametrization can be applied to the aperture and sensor plane.*

4. THE PLENOPTIC CAMERA

Lippmann presented the concept of plenoptic imaging in 1908 [16]. Almost a century later, the concept became increasingly popular and tangible when Ng *et al*. presented a commercially available handheld plenoptic camera in 2005 [6], [8], [15]. To obtain spatial information, an array of microlenses is placed in front of the image sensor [6], [15]. Figure 2 shows the conceptual setup of said cameras. Light emitted from a point on the focal plane D_0 will enter the aperture on different positions [17], wherein we already assume point sources as light emitters. The objective is conceptually equivalent to the one from a normal camera. However, the light is now focused on the microlens array (MLA), not on the sensor [6], [15], [17]. The rays entering the aperture in different positions are now at the same coordinate, yet with different incident angles [6]. As shown in Figure 2, the MLA preserves this angular information. Light rays entering the aperture at different locations will hit a different pixel behind the microlens [6], [15]. The xy-coordinate from Figure 3 is hence given by the intersection of the ray with the MLA. In addition, the uv-coordinate is given by the intersection of the ray with the microlens i.e. the pixel behind this specific microlens (see Figure 4) [5], [6], [8].

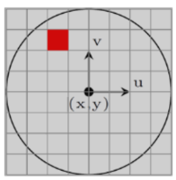

Figure 4*: Coordinates of a microimage. The circle represent the image of the circular aperture by a microlens* [8]**.**

Figure 5 shows a grayscale image of raw sensor data, which was recorded with the Lytro Illum camera used in this work. The microlenses can clearly be seen when zooming in the image. Figure 4 presents the coordinate system for each circular micro-image [8]. In a standard plenoptic camera (e.g. the used Lytro Illum) the distance of the MLA to the sensor equals the focal length of the microlenses [15], [17] (Figure 2). By calibrating the position of the MLA in front of the image sensor it is possible to obtain $L_{D_0}(x, y, u, v)$ directly.

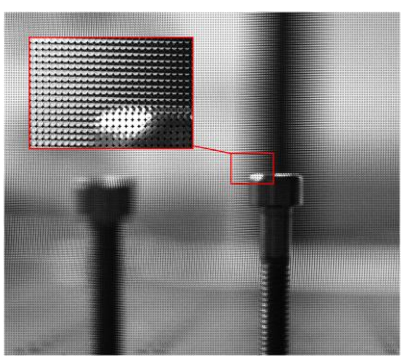

Figure 5*: Plenoptic raw sensor data of 2 bolts.*

5. REFOCUSING AND THREE-DIMENSIONAL INFORMATION

A plenoptic camera allows to refocus an image at different z-coordinates, i.e. at different distances after it has been taken [12], [13], [15], [18]. More detailed explanations of this process well beyond the short description below are provided by Hahne et al. [18] and Ng [15] or Ng [12]. Figure 6 can be interpreted as a side view of Figure 3 and demonstrates the geometrical principle of the used algorithm, which originates from Ng [15]. Refocusing is conducted by calculating the coordinates $\bar{x}, \bar{y}$ a light ray would hypothetically hit at the image sensor, if it originated from a nearer $\alpha < 1$ or further $\alpha > 1$ position, as defined similarly by [7], [15]. Hereby, α is defined by Figure 6 as the scaling parameter of the focal plane distance [15]. Using linear functions and the intercept theorem it can be calculated what the light field would have looked like, if it had been sampled at a different, virtual focal plane by equating [7], [15]:

$$L_{D1}(\bar{x}, \bar{y}, u, v) = L_{D0}(u\left(1 - \frac{1}{\alpha}\right) + \frac{\bar{x}}{\alpha}, v\left(1 - \frac{1}{\alpha}\right) + \frac{\bar{y}}{\alpha}, u, v) \quad (5)$$

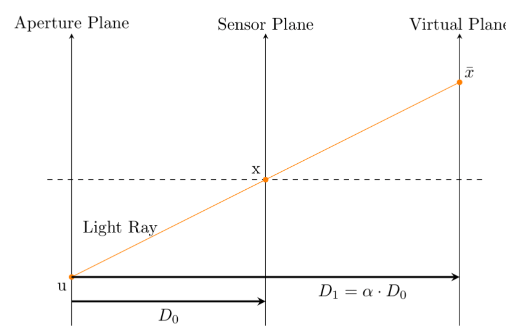

Figure 6: *Refocusing principle. The light field image of a virtual sensor position can be calculated by applying geometrical principles. This 2D representation outlines one spatial coordinate. Adapted from* [12]**.**

As α is continuous it is not given that the calculated coordinates $\bar{x}, \bar{y}$ will fit the previous discrete pixel sampling x,y. It is thus necessary to apply an interpolation to the raw sensor data to get L_{D1} from L_{D0} in the software when carrying out the refocusing procedure [7], [19], [20]. To obtain a refocused photograph, the photography operator (Equation 3) is applied to the shifted light field [7], [15].

6. DEPTH OF FIELD AND EXPECTED RESOLUTION

Imaging resolution in lateral direction is determined by the image sensor and by the optical components of the schlieren system. Using the Lytro Illum, the resolution in xy-plane is approximately 16 px/mm. For an attempted reconstruction also the resolution in z-direction (axial direction) has to be considered. Axial precision of a 3D plenoptic imaging system is strongly determined by the depth of field (DOF) of the camera [10]. The depth of field is usually defined as the distance between the furthest and nearest object that are in sufficient focus [21]. What is acceptable is determined by the size of so-called circle of confusion (CoC) – here we take one pixel size as ‘acceptable’. The narrower the DOF, the higher imaging resolution in z-direction is attainable [5], [10], [22]. The limiting distances of objects in focus are shown in Figure 7 being labeled as P_n and P_f.

Quantitatively, focus can be measured by Graylevel Local Variance (GLLV) [23], [24]. This operator (Equation 6) uses $L_v(i,j)$ which is ``the variance of gray-levels within a neighborhood'' [23] area around (i,j) and the average $\bar{L}_v$. The set of center points Ω herein equates the neighborhood [23], [24].

$$\text{GLLV} = \sum_{i,j\in\Omega(x,y)} (L_v(i,j) - \bar{L}_v)^2 \quad (6)$$

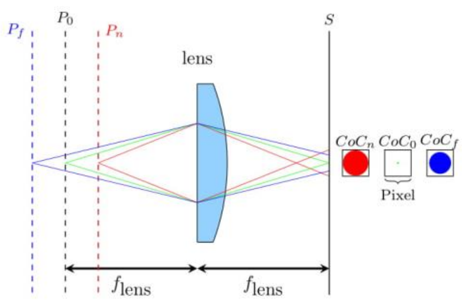

Figure 7: ***Schematic of depth of field for a lens.***

Using approaches from Hahne *et al.* [17], [18] the DOF of the Lytro Illum can be calculated as roughly 210 mm if the lens is set to a focal length of 130 mm and focused at 1500 mm. This initial value is then propagated through the focusing schlieren system. This yields a DOF of 7.5 mm for the whole setup. This is substantially larger than the 2 mm value reported by Ahmed and Wiley [10].

7. THREE DIMENSIONAL RECONSTRUCTION

Levoy et al. [5] describe two inherent ways to measure spatial information by photography: Firstly, to capture the object from different angles, hence a tomographic method. Secondly, to capture the object at various focal lengths, thus a shape-from-focus method [5]. Both are theoretically possible with a plenoptic camera [25]. The MLA provides the possibility to reveal a finite number of different viewing angles with which a tomography approach could be performed [5]–[7]. In addition, the 4D light field can be utilized to obtain different focal planes and therefore a shape-from-focus method could be applied to the plenoptic images [5], [25]. In this work, a 3D deconvolution is performed rather than a tomographic approach. To obtain depth information a focal stack is generated from a single light field image by varying the focus parameter α.

Herein, every focal slice contains blurred light and schlieren information from other focal slices and thus does not only contain information about a single axial depth coordinate [5]. As part of a 3D reconstruction, this out of focus light needs to be removed from the slices in order to reveal the true volume, directly following reconstruction approaches from Levoy et al. [5] developed for microscopy. We assume that the semi-transparent nature of microscopic samples of Levoy et al. [5] to be directly comparable to schlieren deflection signals. An assumption justifiable due to results in Ref. [4]. This means to find the voxel (3D equivalent of a pixel), where the blurred light – from a density gradient - in other focal depths is originally emitted [5]. For this process it is essential to characterize the optical imaging system to be able to estimate the true object.

7.1. The Point Spread Function

As described in Section 6 and shown in Figure 7, a point in object space is only imaged as a point on the camera sensor if it is in focus. A point further away from the focal plane will become spread over several pixels of the sensor and therefore occur blurred in the image. The amount of blur grows proportionally with the distance to the focal plane [21]. If a focal stack of a point is generated, which means imaging a point shaped light source at different focal depths, this will yield a ``double cone'' [5] shaped structure as shown in Figure 8. In positive and negative depth direction the point defocusses to a larger circle of confusion. Due to a limit of resolution which depends on the pixel size, the quality and the nature of the optical components, the double cone’s thickness becomes non-zero at the center and it is thus ``hourglass shaped'' (Figure 8) [5]. This ``hourglass shaped'' [5] 3D structure is the so-called point spread function (PSF) representing the blur a voxel experiences when it is imaged dependent on its position in space relative to the focal plane of the camera [22]. The process of photography can hence be expressed as a convolution of the object V with the PSF creating the light field LF [4], [5]. This light field is then post-processed by the refocusing algorithm to obtain a focal stack, a set of pictures focused at a finite number of depths [5].

$$LF = PSF * V \quad (7)$$

This equation can also be discretized and written as a matrix multiplication. Where H represents the full PSF [22].

$$LF = H \cdot V \quad (8)$$

Even though the PSF may be dependent on the volume [22], for this work the PSF is measured at a single, central point as a preliminary approach. Measuring is done by back illuminating a 5 μm diameter pinhole with a green LED, which is also used for the illumination of the schlieren system. The point source is then recorded with the usual procedure and a focal stack is generated. Figure 8 shows a resulting PSF revealing a typical ``hourglass shape'' [5] providing basic confidence in the methodology.

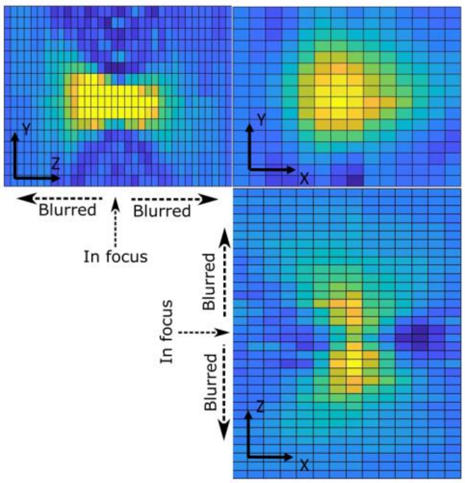

Figure 8: ***Measured point spread function of focusing schlieren computational refocusing process.***

7.2. Reconstruction algorithms

Performing a reconstruction means solving Equation 8 for V which is ideally done iteratively [5], [9]. A constrained iterative algorithm described by M. Levoy et al. [5] is thus modified and used to recover 3D information. We apply a small factor β to reduce the 'strength' of the volume subtraction. The initial guess is obtained by simply removing blur from the slices by applying the Richardson-Lucy iteration scheme [26], [27] which differs from Levoy et al.'s [5] approach. In Equation 9, I represents the measured volume. The second equation expresses the constraint that the volume cannot have negative intensity [5]. The algorithm compares the guess and the measured volume and iteratively corrects the volume by the difference. Based on this principle a reconstruction of 3D structure from plenoptic images is applied to focusing schlieren [5].

$$\Delta^{(k+1)} = I - \beta(V^{(k)} * PSF) \tag{9}$$

$$V^{(k+1)} = \max\left(V^{(k)} + \Delta^{(k+1)}, 0\right)$$

8. EXPERIMENTAL RESULTS

Similarly to Ahmed and Wiley [10], schlieren images are recorded with the focusing schlieren system. In the experimental setup a green LED is used with a diffusor in front of it. The source lens is a 280 mm diameter Fresnel lens with 208 mm focal length. A 85 mm camera lens with f-number 1.4 is used as a schlieren lens and the same horizontal grid pattern is mounted behind the camera lens. The schlieren image is then focused to the camera by a 150 mm aspheric lens. To record the images, multiple options are available. Previously, a Photron high speed camera and Nikon D610 were used to capture schlieren images [28]. The innovation of this work is to add a Lytro Illum plenoptic camera to the system as opposed to Ahmed and Wiley [10] who utilized multiple light sources. It has a focal length of 70-250 mm and a fixed f number of f2.0. The focal range is from 0 mm in front of the camera lens to infinity and is set to 130 mm in the current setup. Its resolution is "40 Megarays" which is a term introduced by Lytro to describe the resolution of the light field. The image sensor is a CMOS ½" (6.4 mm x 4.8 mm). Effectively, the MLA in use is made up of 625 x 433 microlenses. Each microlens spans 15x15 pixels. As a schlieren source a mixture of different Fluoroethanes is used. With a refractive index of $n \approx 1.30$ at room temperature they provide a reasonably strong schlieren sources that can be imaged with the plenoptic camera [29]. The gas is injected into the test section of the focusing schlieren system through transparent tubes measuring 3 mm in diameter and the alignment is shown in Figure 9. Again, we herein roughly follow the approach from Ahmed and Wiley [10] to create reasonably distinguishable 3D objects. One of these tubes has a 0.5 mm diameter transparent thread attached to it, which should mark the depth of the schlieren and also show the maximum reconstruction capacity. The distance of the tubes in z-direction is approximately 34 mm.

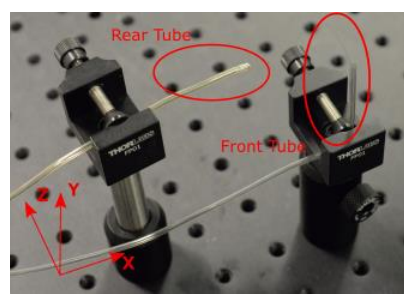

Figure 9*: Tube setup in focusing schlieren test section.*

Images are taken using a Lytro Illum plenoptic camera and Lytro Power Tools version 1.0.0b1 as a camera control software. A general structure for decoding and processing the data was established and is shown in the block diagram in Figure 10. Using the method described in Section 6 the DOF of the setup is determined to be 7.5 mm. As the test section is 250 mm in axial distance it is expected that more than 25 focal slices can be resolved within the object space. This calculation is verified by measuring the depth of field. The GLLV is applied to a focal stack of an optically thick object in the schlieren test section. By comparing the change in blur to the maximum focus yields a measured DOF of 7.2 mm

8.1. Refocusing of Schlieren Images

Figure 11 shows that the application of the refocusing operator is not only valid for optically dense objects such as the tubes, but also for optically thin schlieren objects.

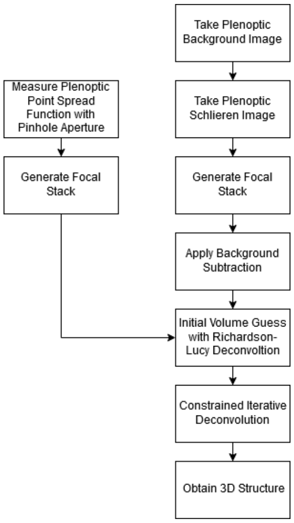

Figure 10*: Workflow for decoding and processing of light field schlieren images.*

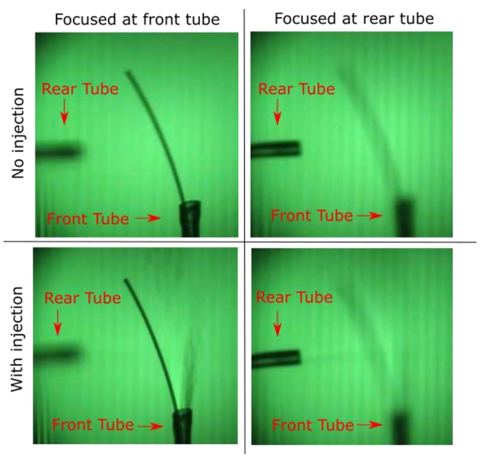

Figure 11: ***Digital refocusing. No gas injection (top), gas injection (bottom).***

Additional optical components of the focusing schlieren system do not affect the ability to rearrange the light field, as it is expected because of previous applications to microscopes [5]. In Figure 12, α is the refocusing parameter from Equation 5 and represents a location along the z-axis. The GLLV focus measure [23], [24] described in Equation 6 was applied to a focal stack. Two maxima are clearly shown in the focus measure, which correspond to the position of the tubes.

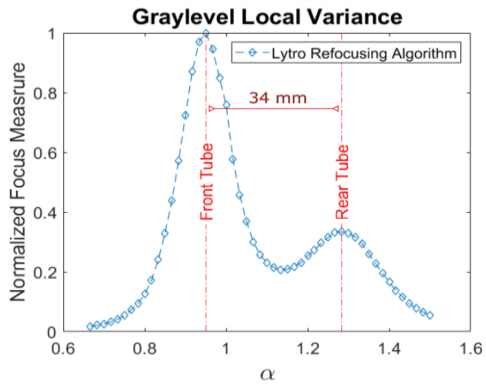

Figure 12: ***Graylevel Local Variance for a focal stack of two tubes.***

It is hence possible to conclude, that the horizontal tube is behind the vertical tube in axial position. This presents the first and most simple 3D information obtained from our plenoptic schlieren system.

8.2. Reconstruction of Schlieren Images

A program structure has been developed in MATLAB using and modifying approaches from Dansereau *et al*. [19], [20] and Prevedel *et al.* [30]. The full program includes processing the Lytro output data files, decoding the raw light field sensor data, aligning the microlens array and finally refocusing (those steps are conducted utilizing the work and code of Dansereau *et al*. [19], [20]) and reconstructing. For the following example of the two tubes, the light field image was firstly background subtracted following the scheme of Figure 10. This is obtained by taking an image without flow injection at the same camera settings and lighting conditions. Due to very low deflection angles in the gas, according to Equation 2, the light signal originating from a density change is comparably low, leading to a small signal-to-noise ratio. Especially hot pixels present a source of defects, which will be amplified by the reconstruction. As only grayscale images are used as an input to the reconstruction a morphological opening [31] is performed to reduce the influence of sensor noise. The effect can be seen in
Figure 13.

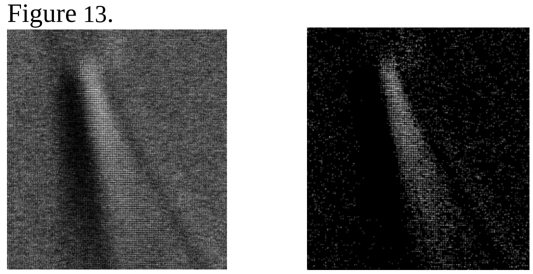

Figure 13: ***Morphological opening. Left, original noisy light field from a schlieren object. Right, morphologically opened image*.**
A focal stack of 51 images is then generated by the program and used as an input for an iterative deconvolution. In this

example the algorithm is a Richardson-Lucy Iteration scheme with 100 iterations. The result from this is used as an input for the algorithm described in Equation 9. Figure 14 shows the xy-view of the reconstructed volume and the resolved objects. The tubes are shown in the reconstruction due to reflection effects. Only the schlieren objects with the highest intensity are being successfully reconstructed by the algorithm. Noise and reconstruction artifacts are present even after the morphological opening of the images and are somewhat intensified by the Richardson-Lucy scheme. We therefore subsequently apply a `cutoff' in intensity and herby remove low amplitude noise. The 3D view is shown in Figure 15 and it has been potentiated by 0.01 to bring most reconstructed objects to a similar intensity value. This does not affect the qualitative 3D structure but aids the depiction and color scheme in Figure 15. The structure in z-direction could clearly be resolved. The position of the front and the rear tube are represented correctly, in addition to the position of the related schlieren sources. It can be seen that the 0.5 mm strand has a smaller extension in z-direction than the tube and the schlieren source. Hence, qualitative statements about length scales in axial direction are represented accurately. It can also be seen that the turbulent part of the rear tube flow is extending in z-direction further away from the tube exit. This is also expected and shows that the schlieren structure is resolved in 3 dimensions.

9. CONCLUSION

This paper showed that the 3D reconstruction of focusing schlieren images from a single photo is possible with a plenoptic camera. We hence explored the opposite setup structure as found in Refs. [10], [11] but still largely followed their approach. Although a direct comparison is difficult, the success with both concepts increases confidence in said plenoptic 3D measurement methodologies in combination with schlieren. This also holds for comparisons to Ref. [4], where no plenoptic camera was used, but other spects of the work are closely related. Nevertheless, it seems as if the high resolution light field data from the plenoptic camera is suitable for a full 3D reconstruction. Schlieren images were recorded with a focusing schlieren system using gas injected from small tubes as schlieren sources. Reconstruction was then performed using and modifying software approaches from different light field and biomedical applications. The results showed valid 3D information for semitransparent schlieren objects and for the respective tubes. However, there are still some remaining challenges such as the perceived elongation of objects in axial direction. As this behavior is similar to results from an example code published by Prevedel *et al*. [30] we expect the problem to be located in the reconstruction algorithm and probably the scaling of the point spread function. A low signal to noise ratio of the schlieren objects complicates the reconstruction. Image enhancement could recover the schlieren signals with comparably high intensity and sufficient levels were achieved to perform a deconvolution but not the entire flow object could be resolved. Thus, it is planned to evaluate the system on stronger schlieren sources such as supersonic shocks, increase the intensity of the light source and further improve the homogeneous lighting conditions as well as the morphological opening procedure. Long term plans for the focusing plenoptic schlieren system are the improvement of the camera technology and an application to hypersonic wind tunnel testing. We ultimately plan to resolve more complex 3D flow effects for example in boundary layers of hypersonic flow from a single photograph.

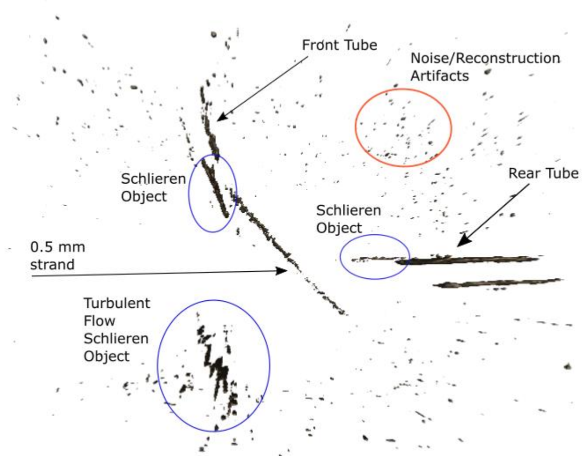

Figure 14: ***XY view of the volume generated with Matlab.***

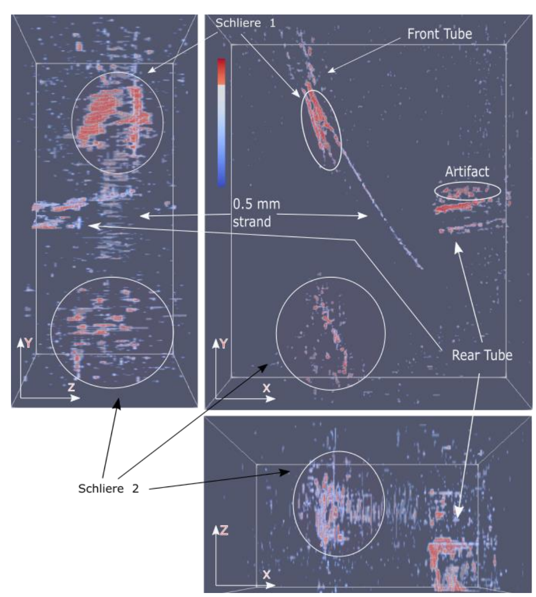

Figure 15: ***3D representation of the obtained reconstruction results. The views were generated with ParaView.***

ACKNOWLEDGEMENTS

The help of Grahame Faulkner with the laser safety risk assessment is gratefully acknowledged. The authors would like to extend their gratitude towards the funding by EPSRC through the transpiration cooling grant EP/P000878/1.

10. REFERENCES

[1] G. S. Settles, *Schlieren and Shadowgraph Techniques*. 2001. doi: 10.1007/978-3-642-56640-0.

[2] L. M. Weinstein, "Large-field high-brightness focusing schlieren system," *AIAA Journal*, vol. 31, no. 7, 1993, doi: 10.2514/3.11760.

[3] A. KANTROWITZ and R. L. TRIMPI, "A Sharp-Focusing Schlieren System," *Journal of the Aeronautical Sciences*, vol. 17, no. 5, 1950, doi: 10.2514/8.1623.

[4] S. Vaisakh and T. M. Muruganandam, "Schlieren Tomography to Visualize Three-Dimensional Supersonic Flows," in *31st International Symposium on Shock Waves 1: Fundamentals 31*, 2019, pp. 421–428.

[5] M. Levoy, R. Ng, A. Adams, M. Footer, and M. Horowitz, "Light field microscopy," in *ACM Transactions on Graphics*, 2006, vol. 25, no. 3. doi: 10.1145/1141911.1141976.

[6] E. H. Adelson and J. Y. A. Wang, "Single Lens Stereo with a Plenoptic Camera," *IEEE Trans Pattern Anal Mach Intell*, vol. 14, no. 2, 1992, doi: 10.1109/34.121783.

[7] T. W. Fahringer and B. S. Thurow, "Tomographic reconstruction of a 3-D flow field using a plenoptic camera," in *42nd AIAA Fluid Dynamics Conference and Exhibit 2012*, 2012. doi: 10.2514/6.2012-2826.

[8] J. N. Klemkowsky, T. W. Fahringer, C. J. Clifford, B. F. Bathel, and B. S. Thurow, "Plenoptic background oriented schlieren imaging," *Meas Sci Technol*, vol. 28, no. 9, 2017, doi: 10.1088/1361-6501/aa7f3d.

[9] M. Eberhart and S. Loehle, "Light field analysis of optically thin plasma flows," in *AIAA Scitech 2019 Forum*, 2019. doi: 10.2514/6.2019-1503.

[10] K. A. Ahmed and A. Wiley, "Structured light-field focusing for flowfield diagnostics," *Exp Therm Fluid Sci*, vol. 89, 2017, doi: 10.1016/j.expthermflusci.2017.08.003.

[11] R. W. Ozawa, J. Reyes, and K. Ahmed, "Structured light-field focusing 3D density measurements of a supersonic cone," in *AIAA Aerospace Sciences Meeting, 2018*, 2018, no. 210059. doi: 10.2514/6.2018-0410.

[12] R. Ng, "Fourier slice photography," in *ACM Transactions on Graphics*, 2005, vol. 24, no. 3. doi: 10.1145/1073204.1073256.

[13] M. Levoy and P. Hanrahan, "Light field rendering," in *Proceedings of the 23rd Annual Conference on Computer Graphics and Interactive Techniques, SIGGRAPH 1996*, 1996. doi: 10.1145/237170.237199.

[14] A. Gershun, "The light field," *Journal of Mathematics and Physics*, vol. 18, no. 1–4, pp. 51–151, 1939.

[15] R. Ng, M. Levoy, M. Bredif, G. Duval, M. Horowitz, and P. Hanrahan, "Light Field Photography with a Hand-held Plenoptic Camera," 2005.

[16] G. Lippmann, "Épreuves réversibles donnant la sensation du relief," *Journal de Physique Théorique et Appliquée*, vol. 7, no. 1, 1908, doi: 10.1051/jphystap:019080070082100.

[17] C. Hahne, A. Aggoun, S. Haxha, V. Velisavljevic, and J. C. J. Fernández, "Light field geometry of a standard plenoptic camera," *Opt Express*, vol. 22, no. 22, 2014, doi: 10.1364/oe.22.026659.

[18] C. Hahne, A. Aggoun, V. Velisavljevic, S. Fiebig, and M. Pesch, "Refocusing distance of a standard plenoptic camera," *Opt Express*, vol. 24, no. 19, 2016, doi: 10.1364/oe.24.021521.

[19] D. G. Dansereau, O. Pizarro, and S. B. Williams, "Linear Volumetric Focus for Light Field Cameras.," *ACM Trans. Graph.*, vol. 34, no. 2, pp. 11–15, 2015.

[20] D. G. Dansereau, O. Pizarro, and S. B. Williams, "Decoding, calibration and rectification for lenselet-based plenoptic cameras," in *Proceedings of the IEEE conference on computer vision and pattern recognition*, 2013, pp. 1027–1034.

[21] N. Salvaggio, *Basic photographic materials and processes*. Routledge, 2013.

[22] M. Broxton *et al.*, "Wave optics theory and 3-D deconvolution for the light field microscope," *Opt Express*, vol. 21, no. 21, 2013, doi: 10.1364/oe.21.025418.

[23] S. Pertuz, D. Puig, and M. A. Garcia, "Analysis of focus measure operators for shape-from-focus," *Pattern Recognit*, vol. 46, no. 5, 2013, doi: 10.1016/j.patcog.2012.11.011.

[24] J. L. Pech-Pacheco, G. Cristóbal, J. Chamorro-Martinez, and J. Fernández-Valdivia, "Diatom autofocusing in brightfield microscopy: a comparative study," in *Proceedings 15th International Conference on Pattern Recognition. ICPR-2000*, 2000, vol. 3, pp. 314–317.

[25] M. Levoy, "Light Fields and Computational Imaging," *Computer (Long Beach Calif)*, vol. 39, no. 8, pp. 46–55, 2006, doi: 10.1109/MC.2006.270.

[26] W. H. Richardson, "Bayesian-based iterative method of image restoration," *JoSA*, vol. 62, no. 1, pp. 55–59, 1972.

[27] L. B. Lucy, "An iterative technique for the rectification of observed distributions," *Astron J*, vol. 79, p. 745, 1974.

[28] H. S. Ifti, T. Hermann, and M. McGilvray, "Flow characterisation of transpiring porous media for hypersonic vehicles," in *22nd AIAA International Space Planes and Hypersonics Systems and Technologies Conference*, 2018. doi: 10.2514/6.2018-5167.

[29] "https://www.parchem.com/chemical-supplier-distributor/Ethyl-Fluoride-087673.aspx," Aug. 06, 2019.

[30] R. Prevedel *et al.*, "Simultaneous whole-animal 3D imaging of neuronal activity using light-field microscopy," *Nat Methods*, vol. 11, no. 7, p. 727, 2014.

[31] L. Vincent, "Morphological area openings and closings for grey-scale images," in *Shape in Picture*, Springer, 1994, pp. 197–208.

[32] F. Wechsler, "Wavefront Coding Techniques for Extended Depth of Field in Light Field Microscopy," 2018.